J Sol-Gel Sci Technol (2016) 79:520–524
DOI 10.1007/s10971-016-4065-5

BRIEF COMMUNICATION: SOL-GEL AND HYBRID MATERIALS FOR OPTICAL, PHOTONIC AND OPTOELECTRONIC APPLICATIONS

Visible wavelength-independent anti-reflection coatings generated from assembled SiO_2 particles modified with tetraethoxysilane

Lei Yang[1,2] · Hui Jiang[1] · Xiaolei Feng[2] · Yifeng Shen[1,2] · Longlong Jia[2]

Received: 21 December 2015 / Accepted: 6 May 2016 / Published online: 13 May 2016

Abstract The objective of this research was the fabrication of visible wavelength-independent anti-reflection coatings by deposition and aggregation of silica nanoparticles. This approach to anti-reflection coatings is important for technologies which avoid sophisticated process and calcination at high temperature. The goal of this research was achieved by modification of a commercially available SiO_2 dispersion with tetraethoxysilane (TEOS) and spin coating of the TEOS–SiO_2 (T–SiO_2) dispersion. The modification resulted in aggregation of T–SiO_2 particles upon evaporation of ethanol aqueous solution and thus assembled into many enlarged bulges at the coating surface. The resulted coating surface morphology resembled moth-eye-like nanostructure that exhibited visible wavelength-independent transmittance enhancement for substrate. More promisingly, owing to this unique behavior, the coated colored substrates display deepened colors without sacrificing any color hues. Such coating is very attractive in many fields such as color displaying and color imaging.

Graphical Abstract

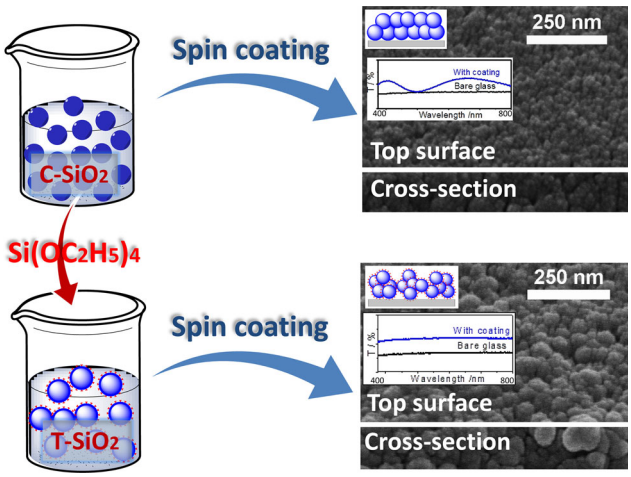

Keywords Anti-reflection coating · Visible wavelength-independent · Sol–gel · Deepening color · Silica nanoparticles

1 Introduction

Reducing unwanted reflections plays a pivotal role in many applications such as flat-panel displays, photodetectors, infrared sensors and lenses [1]. A reduction in one specific wavelength reflection is typically accomplished by coating of an anti-reflection layer with a quarter-wavelength optical thickness [2]. However, since the enhancement of transmittance is selective toward specific wavelengths, the coating exhibits a high transmittance only in a narrow wavelength range and destroys the real color [3]. As such, broadband anti-

Electronic supplementary material The online version of this article (doi:10.1007/s10971-016-4065-5) contains supplementary material, which is available to authorized users.

✉ Lei Yang
yanglei@zstu.edu.cn

[1] Key Laboratory of Advanced Textile Materials and Manufacturing Technology, Ministry of Education, College of Materials and Textiles, Zhejiang Sci-Tech University, Hangzhou 310018, Zhejiang, China

[2] Engineering Research Center for Eco-Dyeing and Finishing of Textiles, Ministry of Education, College of Materials and Textiles, Zhejiang Sci-Tech University, Hangzhou 310018, Zhejiang, China

reflection coatings especially with visible wavelength-independent spectra are highly desired to achieve an optimal performance, like real-color reproduction.

To date, two techniques, namely constructing multilayer coating [4] and fabricating a layer with moth-eye-like structure [5], have been designed to prepare broadband anti-reflection coatings. In comparison with multilayer coating, the coating with moth-eye-like structure may display higher transmittance over a wide range of wavelength and incidence angles [6]. Versatile innovative techniques have been devised to mimic the structure of moth eyes such as lithography, etching and sol–gel method [7].

Among the above-mentioned techniques, the sol–gel method may be the most promising one due to its remarkable advantages of low cost, simple operation process and extensive applications [8]. As the coatings were prepared, sol–gel nanoparticles with round contour could form many bulges on the coatings once they covered the coating surface. The resulted surface morphology resembled the structure of moth's eye, which caused the gradient in refractive index between air and coating surface and prevented the light reflecting off the coating surface. Particle size was important for the anti-reflective performances of the coatings. Anti-reflection coating prepared from SiO_2 particles with diameters in the range of 3–20 nm show noticeable wavelength-dependent transmittance enhancement [9]. On the contrary, enhanced transmittance exhibiting nearly visible wavelength-independent character was observed for coatings composed of mesoporous silica nanoparticles with diameter of around 130 nm [10]. However, calcination of the spin-coated films was essential for the formation of mesoporous structure, which limited their applications.

In this study, we reported a way to fabricate moth-eye-like anti-reflection coating through aggregation of small SiO_2 particles. A commercially available 20-nm SiO_2 particle (C–SiO_2) was modified by tetraethoxysilane (TEOS) and was then used for casting of anti-reflection coatings on quartz slides. The modification caused TEOS–SiO_2 (T–SiO_2) to form aggregates during casting and thus enlarged bulges at the coating surfaces. The effects of surface morphologies on transmission spectra of the anti-reflection coatings were investigated. In addition, the influence of the anti-reflection coatings on the absorption spectra of the colored substrates was evaluated.

2 Experiment

2.1 Preparation of coatings

Both C–SiO_2 and T–SiO_2 coatings were produced on clean quartz glass slides by a spin-coating process. The spinning speed was maintained at 800 rpm for the first 9 s and increased to 2000 rpm for another 40 s. Then, the coated substrates were heated at 160 °C for 8 h. Prior to spin coating, the C–SiO_2 dispersion (30 wt% silica and 70 wt% water, pH = 7.1, Zhejiang Yuda Chemical Co. Ltd.) was diluted with absolute ethanol to 5 wt%. So, the mass composition of C–SiO_2 coating solution is water/ethanol/silica = 11.7/83.3/5.0. The T–SiO_2 dispersion for spin coating was prepared as follows: 33.3 g of C–SiO_2 dispersion was added into a mixture of 65.7 g of absolute ethanol and 1.0 g of TEOS. The dispersion was stirred at room temperature for 24 h. Finally, the resulting T–SiO_2 dispersion was diluted with 100 g of absolute ethanol to 5 wt%. To evaluate the color deepening effects of the silica coatings, quartz slide was evenly deposited with colors onto one side via ink jet printing. After that, the other side of the slide was spin-coated with silica.

2.2 Characterization

Chemical composition of C–SiO_2 and T–SiO_2 was analyzed by X-ray photoelectron spectroscopy (XPS, K-Alpha Thermo Fisher Scientific) and Fourier transform infrared spectroscopy (FTIR, Nicolet 5700) using KBr pellet method, respectively. The particle morphology of C–SiO_2 and T–SiO_2 was observed by transmission electron microscopy (TEM, JSM-1200 EX T20). Zeta potential was measured by dynamic light scattering (DLS, Malvern Zetasizer Nano S). During zeta potential analysis, the mass composition of silica sample was water/ethanol/silica = 90/9.0/1.0. The morphologies of surface and cross section of the coatings were investigated by atomic force microscopy (AFM, XE-100E) and field emission scanning electron microscope (FE-SEM, Ultra55). The light transmission spectra were measured by UV–Vis spectroscopy (Shimadzu UV 2600 spectrophotometer). Color strength (*K/S*) measurements were performed on a Datacolor spectrophotometer (SF600-PLUS) with an integrating sphere. During the measurements, light that enters the sphere from the light source reflects off the coated interior surface of the integration sphere and strikes the sample from all angles. The optical path diagram is schematically shown in Figure S1.

3 Results and discussion

3.1 Characterizations of C–SiO_2 and T–SiO_2

FTIR spectra of the C–SiO_2 and T–SiO_2 are shown in Fig. 1a. The absorption peaks belonging to stretching modes of Si–O–Si bands at 1120 and 805 cm^{-1} and belonging to the hydroxyl group of ≡Si–OH at 955 cm^{-1}

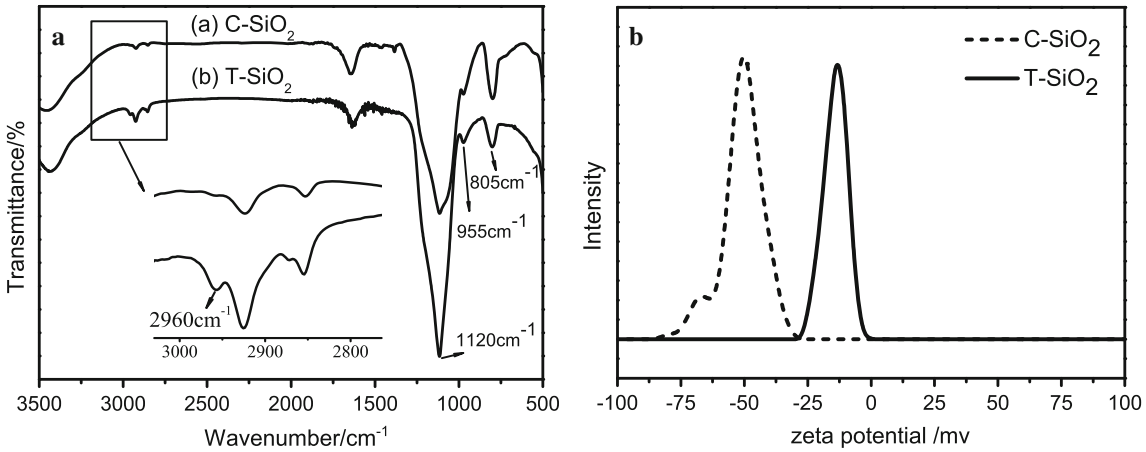

Fig. 1 **a** FTIR spectra and **b** zeta potential of C–SiO_2 and T–SiO_2

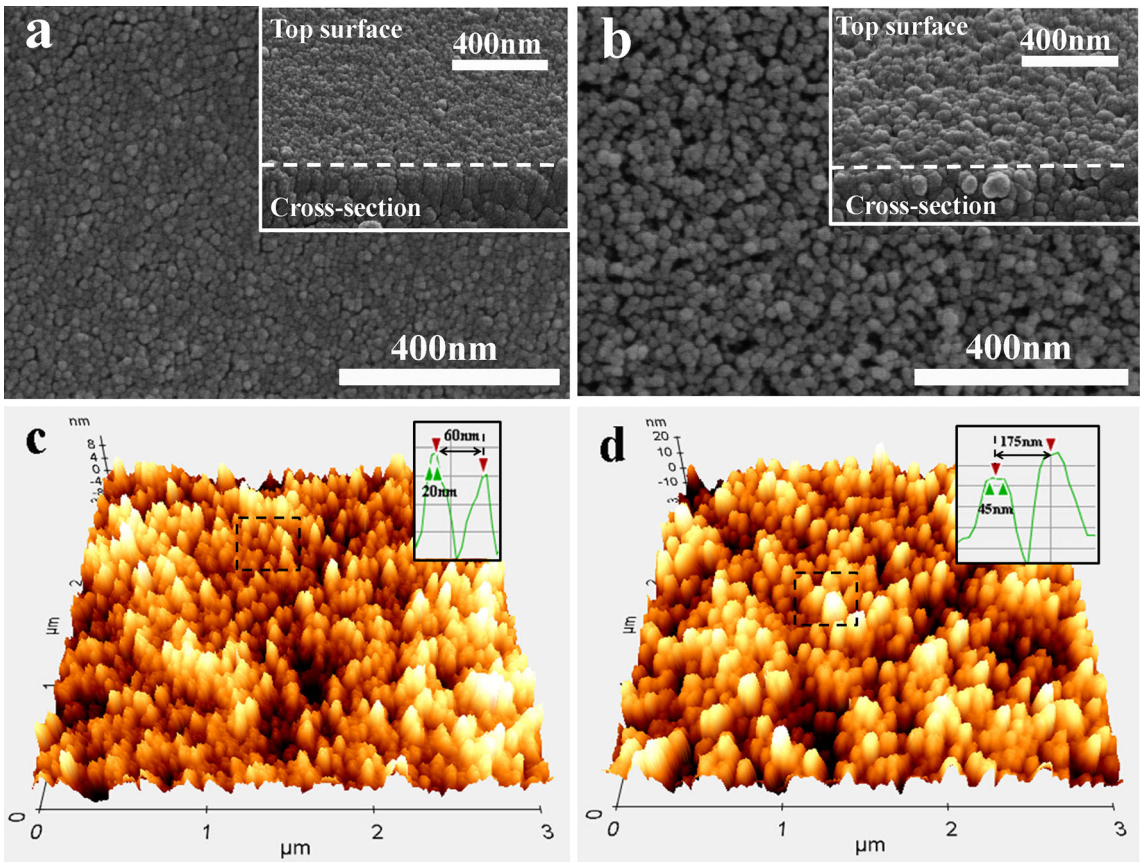

Fig. 2 SEM and AFM images of the C–SiO_2 coating (**a**, **c**) and T–SiO_2 coating (**b**, **d**)

appear in the spectra of both samples. A small additional absorption band at 2960 cm^{-1} appears in the spectrum of T–SiO_2, which could be assigned to the C–H stretching vibration mode (Fig. 1a inset). It indicates that the ethoxy segments originated from TEOS were covalently linked to C–SiO_2 particles. The attachment of ethoxy segments is further confirmed by XRD results shown in Fig. S2, which results in an increase in carbon element content. The intensity ratio of C 1*s*:Si 2*p* increases from 0.13 for C–SiO_2 to 0.23 for T–SiO_2. TEM images in Fig. S3 indicate no significant difference in morphologies between C–SiO_2 and T–SiO_2 particles. These two samples have almost the same particle size of 20 nm. As shown in Fig. 1b, the zeta potential of C–SiO_2 is in the range of −82 to −29 mV. It is

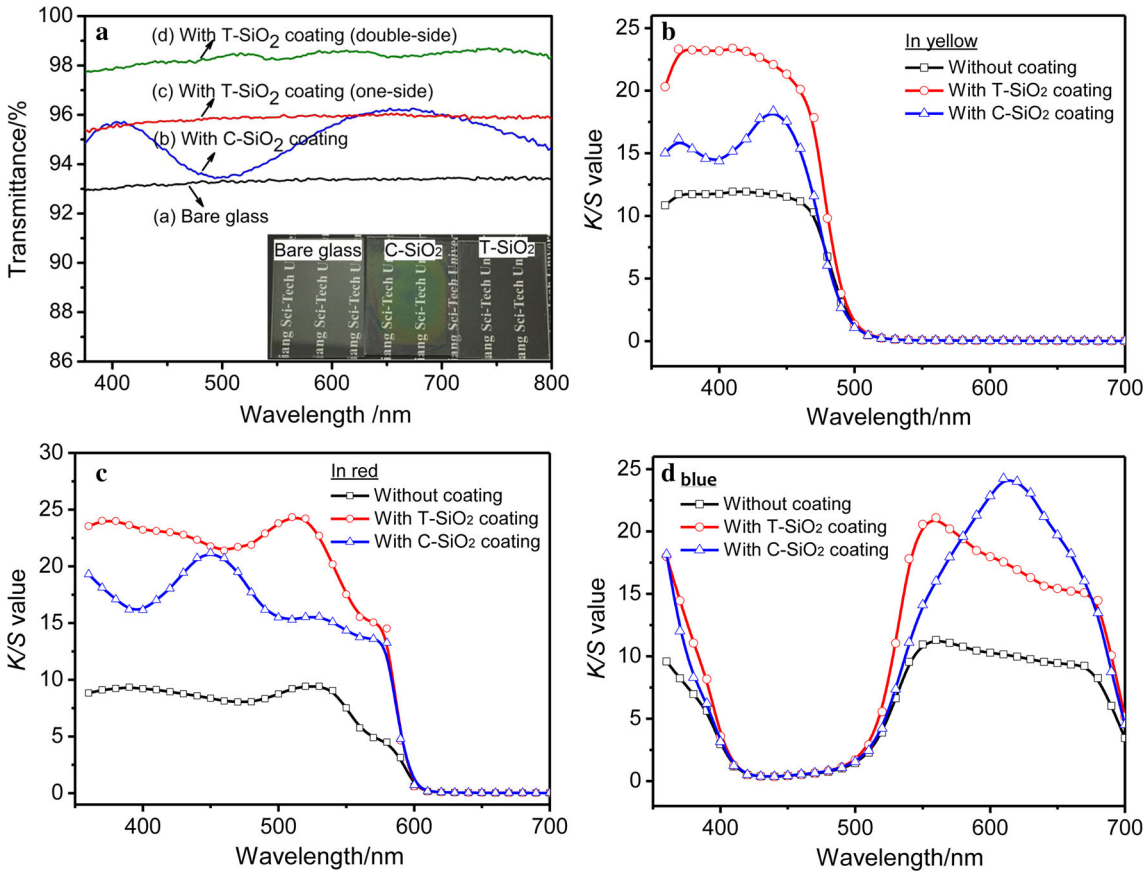

Fig. 3 Effects of C–SiO_2 and T–SiO_2 coatings on transmission spectra (**a**) and *K/S* curves of colored quartz slides in *yellow* (**b**), in *red* (**c**) and in *blue* (**d**). The *inset* in (**a**) shows image of substrate under *bright light*: (1) bare quartz glass, (2) C–SiO_2 coated substrate, (3) T–SiO_2 coated substrate (Color figure online)

increased to the range of −24 to −4 mV for T–SiO_2, probably due to the attachment of non-charged ethoxy segments on the particle surfaces. Therefore, T–SiO_2 would receive weakened electrostatic stabilization owing to its less negative charge. Compared with C–SiO_2, T–SiO_2 may more easily undergo agglomeration to form large aggregates with the evaporation of ethanol aqueous solution in the drying process of coatings [11].

3.2 Surface morphologies and transmittance

The thicknesses of the C–SiO_2 and T–SiO_2 coatings are similar, ca. 1.1 um (Fig. S4). A significant difference is observed between these two coatings in their surface morphologies. As shown in Fig. 2a, the C–SiO_2 particles are homogenously and compactly distributed in the coating, and no obvious aggregation of C–SiO_2 particles is observed. In contrast, a large amount of aggregates of T–SiO_2 particles are observed in the T–SiO_2 coating (Fig. 2b), which could be reasonably ascribed to the weakened colloidal stability caused by the lower surface charge of T–SiO_2 particles. In addition, the aggregates of T–SiO_2 particles are loosely distributed in the coating, leading to the formation of a rough surface. As shown by the tilt SEM images in the insets of Fig. 2a, b, random arrays of bulges formed at air-coating interfaces where C–SiO_2 bulges have much smaller size than those of T–SiO_2. These observations are confirmed by AFM. As revealed in Fig. 2c, d, C–SiO_2 bulges display an average top width (TW) of 20 nm and a spacing of around 60 nm, while the T–SiO_2 bulges show an average TW of 45 nm and a spacing of around 175 nm. The differences in the morphology and dimension of nanostructure could greatly affect the optical properties of coatings [12].

Figure 3a shows the transmission spectra of the bare quartz glass slide and the quartz glass slides covered by the C–SiO_2 and T–SiO_2 coatings. The transmittance of the bare glass slide levels off at around 93 % in the entire visible region (400–800 nm). By comparison, the C–SiO_2 coated slide displays a higher transmittance with wave characteristics. The transmittance exhibits a maximum value of around 96 % at 400 and 660 nm and a minimum value of 93.3 % at 500 nm. The transmittance of quartz glass slide is further enhanced through T–SiO_2 coating. As shown in Fig. 3a, curves with 96 and 98 % transmittance are observed for slides with one-side and double-side T–SiO_2

coatings, respectively. In comparison with the nearly flat curve of one-side coated substrate, weak interference patterns were observed for the double-side coated substrate. However, both samples exhibit broadband anti-reflection performance within the visible wavelength region. According to film optical theory [13], the multi-peak spectral profile manifests the multilayer structure of the C–SiO_2 coating, while the broadband anti-reflection performance together with the surface morphology suggests the moth eye nanostructured array of the T–SiO_2 coating. The optical properties of T–SiO_2 coatings appeared stable over at least a period of several months when the ambient relative humidity was between 60 and 90 %. As shown in Fig. S5, a preliminary test indicated that the coated quartz slide only showed a slight decrease of 0.3 % in transmittance after six months, presumably due to water condensation within the pore structure of the coating. Furthermore, the transmittance enhancement behavior of T–SiO_2 coating depended insignificantly on the storage time of coating solutions. Figure S6 shows that the coatings obtained 60 days after the synthesis of coating solution attained nearly the same anti-reflection performance as the one prepared with freshly synthesized solution.

The inset in Fig. 3a shows bare quartz glass slide, C–SiO_2 and T–SiO_2 coated slides exposed to bright light. The words could be clearly seen through the coated substrates because of the high-quality transparency due to the suppression of reflection, while the words below uncoated one are hazy due to the light reflection. A closer examination revealed that the C–SiO_2 coated surface showed iridescence, which might greatly affect the color imaging.

3.3 Color deepening effects on colored substrates

Three pieces of colored quartz slides in yellow, red and blue were one-side coated with C–SiO_2 and T–SiO_2, respectively. In these cases, the color performance of the coated quartz slides was expected to be determined by the reflection of the coatings and selective light absorption of colorants, simultaneously. The color appearance of slides with coatings was evaluated through *K/S* measurement (*Note*: *K/S* value expresses the color strength as $K/S = (1 - R)^2/2R$, where *R* represents the reflection coefficient.). As indicated by the increased *K/S* peak values shown in Fig. 3b–d, more than 70 % growth of color strength was observed for all samples after being coated with either C–SiO_2 or T–SiO_2. However, due to the wavelength-dependent transmission spectra, the shifts of peak wavelength (λ_{peak}) are observed for the C–SiO_2 coated samples, demonstrating the loss of the original color hues. By contrast, benefiting from the wavelength-independent anti-reflection feature, the shapes of the *K/S* spectra as well as the λ_{peak}s are barely changed in the samples coated by T–SiO_2. This color reproduction character of the T–SiO_2 coating is pivotal for applications of anti-reflection coatings in the fields of color imaging and displaying devices.

4 Conclusions

In this work, a broadband anti-reflection coating was fabricated through a spin-coating process of TEOS-modified commercial SiO_2. The attached TEOS segments slightly weakened the colloidal stability of T–SiO_2. Therefore, the T–SiO_2 particles were inclined to form particle aggregates during the coating process and subsequently to form larger bulges at the coating surfaces. The moth-eye-like surfaces endowed the coatings with increased transmittance being independent on the wavelength over the whole visible region. Thus, after being coated with T–SiO_2, colored substrates exhibited deepened color remaining in their original color hues.

Acknowledgments This project is financially supported by Zhejiang Provincial Natural Science Foundation of China (LY15E030013), Zhejiang Provincial Public Welfare Technology and Application Research Project (2016C31074), Young Researchers Foundation of Zhejiang Provincial Top Key Academic Discipline of Chemical Engineering and Technology (ZYG2015002), Zhejiang Xinmiao Talent Project (2015R406030) and ZSTU innovative research projects for graduate students (YCX14008).

References

1. Schallenberg UB (2006) Appl Opt 45:1507–1514
2. Heavens OS (1955) In Chapter 7 "Practical applications of thin films in optics": optical properties of thin solid films. Dover Publications, New York, pp 207–210
3. Li X, Gao JP, Xue LJ, Han YC (2010) Adv Funct Mater 20:259–265
4. Musset A, Thelen A (1970) In chapter 4 "Multilayer antireflection coatings". In: Wolf E (ed) Progress in optics 8. North Holland Publishing Company, Amsterdam, pp 203–237
5. Clapham PB, Hutley MC (1973) Nature 244:281–282
6. Huang YF, Chattopadhyay S, Jen YJ, Peng CY, Liu TA, Hsu YK et al (2007) Nat Nanotechnol 2:770–774
7. Raut HK, Ganesh VA, Nair AS, Ramakrishna S (2011) Energy Environ Sci 4:3779–3804
8. Chen DG (2001) Sol Energy Mater Sol Cells 68:313–336
9. Zhang X, Cao C, Xiao B, Yan L, Zhang Q, Jiang B (2010) J Sol–Gel Sci Technol 2010(53):79–84
10. Zhang L, Lu CL, Li YF, Lin Z, Wang ZH, Dong H et al (2012) J Colloid Interface Sci 374:89–95
11. Vorotilov K, Petrovsky V, Vasiljev V (1995) J Sol–Gel Sci Technol 5:173–183
12. Ji S, Song K, Nauyen TB, Kim N, Lim H (2013) ACS Appl Mater Interfaces 5:10731–10737
13. Yoldas BE (1980) Appl Opt 19:1425–1429